

The theory of vibrational wave movement in drying grain mixture

V. Bulgakov¹, I. Holovach¹, S. Kiurchev², S. Pascuzzi³, M. Arak⁴, F. Santoro³,
A.S. Anifantis³ and J. Olt^{4,*}

¹National University of Life and Environmental Sciences of Ukraine, 15 Heroyiv Oborony Str., Kyiv UA 03041, Ukraine

²Dmytro Motorny Tavria State Agrotechnological University, 18B Khmelnytsky Ave, UA 72310, Melitopol, Zaporozhye Region, Ukraine

³University of Bari Aldo Moro, Department of Agricultural and Environmental Science, Via Amendola, 165/A, IT70125 Bari, Italy

⁴Estonian University of Life Sciences, Institute of Technology, 56 Kreutzwaldi Str., EE51006 Tartu, Estonia

*Correspondence: jyri.olt@emu.ee

Abstract. This paper outlines a theory that involves the vibrational wave transportation of bulk grain during the course of passing that grain under an infrared radiation source, in a working thermal radiation drying chamber, and using a vibrational wave transporter belt that has been developed by the authors of this paper. The main outstanding feature of the proposed design is the presence of mechanical off-centre vibration drives which generate the vibration in the working rollers at a preset amplitude and frequency, thereby generating a mechanical wave on the surface of the flexible transporter belt which ensures the movement of bulk grain along the processing zone which itself is being subjected to infrared radiation. A calculation method was developed for the oscillation system that is used in conjunction with the vibrational transportation of the grain mass, in order to be able to determine the forces that may be present in the vibrational system and to prepare the differential calculations for the movement of the vibrational drive's actuators, utilising for this purpose Type II Lagrange equations. The solving of the aforementioned integral equations on a PC yielded a number of graphical dependencies in terms of kinetic and dynamic parameters for the vibrational system described above; the analysis of those dependencies provided a rational structural, along with kinetic and dynamic indicators. According to the results that were taken from theoretical and experimental studies on the functioning of the developed infrared grain dryer combined with a vibrational exciter, stable movement for its working roller takes place if the angular velocity of a drive shaft is changed within the range of between 50–80 rads^{-1} , whereas the amplitude of the indicated oscillations falls within the range of 3.0–4.0 mm. It has been discovered that a rational speed when transporting soy seeds during infrared drying falls between the range of between 0.15–0.60 cm s^{-1} , whereas the amplitude of the indicated oscillations falls within the range of 3.0–4.0 mm. An increase of this parameter within the stated limits increases the time that it takes to achieve the stage in which a constant drying soy speed is reached by more than 2.5 times (from 205 seconds to 520 seconds), stabilising the figure at a level of 520 seconds, which makes it possible to recommend a range of transport speeds of between 0.15–0.40 cm s^{-1} under infrared radiation for the seeds in order to achieve the required moisture content with a single pass of the produce on the wave transporter.

With that in mind, the power consumption levels for the vibrational exciter do not exceed 50W, while the angular velocity of the drive shaft's rotation falls within the range of between 100–120 rads^{-1} . The results of the experimental study that has been conducted indicated that a rational transportation speed for the soy seeds on the wave transporter under infrared radiation is between 0.15–0.40 cm s^{-1}

Key words: drying, grain, kinetic and dynamic parameters, model, quality, transportation.

INTRODUCTION

The drying of cereal and oil crop seeds holds an important place in the technology that covers their processing and storage. The use of high-performance grain dryers significantly shortens the time needed to prepare the seeds for long-term storage, while also reducing losses, and creating the necessary conditions for further processing.

On the other hand, the preparation of seeds for long-term storage and subsequent sowing requires significant consumption of heat and mechanical energy. There are currently a good many different designs of dryer in use.

The convective dryer, which is widely used worldwide, has significant shortcomings, such as the fact that the evaporation of moisture from the material that is being processed takes place rather slowly. Drying by means of thermal radiation (under an infrared radiator) eliminates that shortcoming thanks to its ensuring the coincidence of the heat beam's gradient and the material's moisture content which, together with the high energy absorption levels, makes sure this process has one of the best outcomes of all of the methods to be used when intensifying the bulk's heat transfer.

The only limitation in drying by means of thermal radiation is the transparency of the layer of seeds for the infrared radiation, ie. the radiation must penetrate the entire layer, for which purpose the layer's thickness must not exceed a depth of 15mm.

The best method for ensuring the necessary layer thickness of the material that is being dried and its movement along the working area is the use of vibrating technology in the course of the drying process.

But, in our opinion, the best outlook is displayed by thermal radiation dryers with infrared technology, as used in the process of drying grain and seed material. And yet the bulk grain needs to be moving along the drying chamber's working area while it undergoes the process of infrared irradiation of the bulk.

The drying of agricultural materials, in particular grain, requires constant transportation. Therefore the use of belt, conveyor, screw, or other types of transporter is not entirely suitable. Upon ordinary transportation, bulk grain does not become mixed; in addition, such transporters need more metal and energy to make and operate.

Therefore, nowadays the method used in vibrational transportation is also widely used in the transportation of various bulk materials while drying them. There are a number of vibrational transporter designs in use for this purpose, all of which ensure the effective vibrational transportation of bulk grain. For example, in machines which employ a process of constant vibration, a vibrating belt conveyor is used as the transportation element of the design, providing for guaranteed movement of the bulk material. Despite this popularity, all of the aforementioned designs of vibration equipment have significant shortcomings.

Therefore, we have developed a thermal radiation dryer which employs a somewhat novel design, one which uses a vibrational wave transporter belt that moves the bulk grain through the drying chamber's working area in which infrared irradiation and therefore the drying of the bulk grain all takes place. It must be noted that the belt conveyor itself remains stationary (not performing a translational movement); the bulk material is shifted only by a mechanical wave that is generated along its elastic belt by means of vibrational exciters.

Figure 1 provides an overall view of the developed thermal radiation dryer and its novel design which uses a vibrational wave transporter belt (a), and a diagram of its technological design (b).

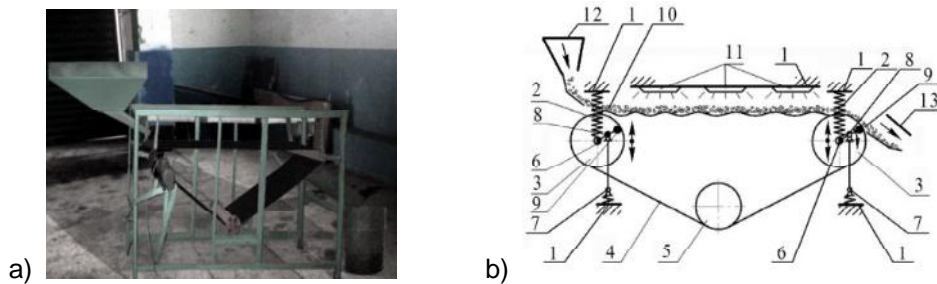


Figure 1. Infrared dryer with a vibrational wave transporter belt: a – overall view; b – technological diagram: 1 – frame; 2 – elastic elements; 3 – rollers; 4 – elastic belt; 5 – tensioning cylinder; 6 – roller axes; 7 – vibration dampers; 8 – off-centre drive shafts; 9 – counterweights; 10 – bulk grain; 11 – infrared radiator; 12 – feeder; 13 – receiving hopper.

The main benefits in using this dryer are its simple design, reliable functioning, and low energy consumption for its operation.

The infrared dryer with its vibrational wave transporter belt has the following design features: the frame (1) houses two vibrational exciters in the form of rollers (3) which are installed onto shafts (6) that are connected to the frame (1) via elastic elements (2). These two rollers (3), installed at the same level as each other, are surrounded by an elastic belt (4). The elastic belt has a horizontal section at the top, between two rollers (3), and a tensioning cylinder (5) at the bottom; the cylinder pulls the belt down under gravity due to its own weight, thereby generating preliminary tensioning in the horizontal top part of the belt.

The insides of the rollers (3) are penetrated by the off-centre drive shafts (8), which have attached counterweights (9) on the outside of one of the side elements of the rollers. The off-centre drive shafts are installed on the frame with the aid of vibration dampers (7). This way, the off-centre drive shafts are connected to the frame via the vibration dampers at the bottom and to the frame via axes (6) and elastic elements (2) at the top. The counterweights (9) offset the inertial forces emerging while the rollers work. Upon the off-centre drive shafts (8) within the rotating rollers, each shaft (3) produces vibrational movement that, if certain parameters have been selected regarding frequency and amplitude, makes it possible for each roller to generate a dynamic wave on the surface of the elastic belt (4) (in the form either of a standing or running wave). This makes it possible to transport the seed bulk (10), but also to mix its layers, and to dry the seed bulk in the working area of the infrared radiator (11). Moreover, when varying the

vibration parameters of the two vibrational exciters in the form of the rollers, the speed of movement of the seed bulk that is coming from the feeder (12) in the working area and the intensity of its mixing can both be changed. Thereafter, the dried seed bulk (10) is moved via vibrational waves into the receiving hopper (13) at the transporter's other end.

In this way, when employing vibrational wave transportation for seed bulk, the bulk is also loosened due to the forces being applied to it by means of their alternating directions, leading to a decrease in the bulk's internal friction and viscosity, as well as to its uniform thermal treatment.

The infrared dryer that has been developed for bulk grain, using a vibrational transporter, is a combination of a belt transporter (without the translational movement of the transporter belt) and a vibration machine with a combined kinetic manner in which it is able to generate oscillations. It establishes the conditions for constant movement and the simultaneous infrared treatment of the continually-fed seed bulk, ensuring its loosened state and guaranteed its drying. This is accompanied by a reduction of the oscillating mass of the vibration drive.

By means of this method - using the equipment that has been developed and which is now being proposed by us - with its two vibrational exciters, it becomes possible to reduce the oscillating mass of the entire drive and provides the levelling of any unwanted oscillations by means of the incorporated flexible elements. This type of design for a drive unit, together with a wave transporter with a deforming transportation element, makes it possible to provide a significantly improved system for balancing the dryer's vibrational drive.

Therefore the implementation of the proposed design for a vibrational dryer with its kinetic method of providing vibrational excitation provides a significantly increased intensive process for removing free and physically-bound moisture from the fed seed bulk on account of having creating a pseudo-levitating state of the material that is being processed, and also makes it possible to ensure lower stress levels in the equipment and lower costs, as well as ensuring the conditions for the effective balancing of the oscillation system.

An analysis of various methods being used in the process of drying cereal and oil crops is provided in previous papers (Boyce, 1965; Safarov, 1991; Bruce & Giner, 1993; Malin, 2005; Moroz et al., 2011; Aboltins & Upitis, 2012; Hemis et al., 2012; Rudobashta et al., 2016; Gilmore et al., 2019; Giner, 2019; Kliuchnikov, 2019; Rugovskii et al., 2019), where the basis for classifying these methods is the one that involves the transferral of heat to the material that is being dried. The convective dryer, which is widely used worldwide, has significant shortcomings, such as the fact that the evaporation of moisture from the material that is being processed happens rather slowly. Drying by means of thermal radiation (under an infrared radiator) eliminates that shortcoming thanks to its ensuring the coincidence of the heat beam's gradient and the material's moisture content which, together with the high energy absorption levels, makes sure this process has one of the best outcomes of all of the methods to be used when intensifying the bulk's heat transfer.

The method used in drying plant materials utilising short-wave infrared radiation is presented in previous papers (Filonenko & Grishin, 1971; Bezbakh & Bakhmutyan, 2006). The only limitation in drying by means of thermal radiation is the transparency of the layer of seeds for the infrared radiation, ie. the radiation must penetrate the entire layer, for which purposes the layer's thickness must not exceed a depth of 15mm.

The best method for ensuring the necessary layer thickness of the material that is being dried and its movement along the working area is the use of vibrating technology in the course of the drying process.

The problem of creating a high-performance drying unit is discussed in previous papers (Goncharevich & Frolov, 1981; Grochowski et al., 2004; El Hor et al., 2005; Palamarchuk et al., 2018), which present the mathematical model for the drying processes, along with the results of experimental studies, the design diagrams for wave-based and vibrational transportation equipment, and proof that one of the most effective methods of intensifying the processes that have been studied is the use of a vibrational field.

The goal of the paper is to increase the productivity and quality in terms of drying the grain and seeds of various crops by means of developing and scientifically reasoning out the rational parameters of a new type of thermal radiation dryer.

MATERIALS AND METHODS

For a theoretical description of the vibrational wave-based movement of bulk grain in the dryer that has been developed by us, it is first necessary to discuss the functioning of the kinetic vibrational exciter which serves to generate the oscillations in an elastic belt, and which effects the process of wave-based movement in the bulk grain that is fed onto it from one end.

First of all, based on the technological design diagram for the thermal radiation dryer with its vibrational transporter belt (Fig. 1), and on the description of its functioning that has been provided above, it is necessary to develop a calculation diagram for the kinetic vibrational exciter that is to be used with the elastic transporter belt's oscillations in its initial position (in a balanced state) and, thereafter, in any of its working positions, ie. when offsetting the work roller's centre of mass from its balanced state. The relevant calculation diagrams are presented in Figs 2 and 3.

The diagram in Fig. 2 indicates these parameters for the oscillating system: m_1 – is the drive shaft's mass; m_2 – is the roller's mass; m_3 – is the counterweight's mass; C_1 – is the elastic support's rigidity levels; C – is the vibration damper's rigidity levels; e – the offset from centre, which is defined by distance $l_{12} = O_1O_2$; $l_{13} = O_1O_3$ – the distance from a drive shaft (point O_1) to a counterweight's axis (point O_3).

For further study of the movement of the oscillating system being discussed, we shall establish an equivalent diagram which indicates the offset for a roller's centre of mass from the balanced state when carrying out

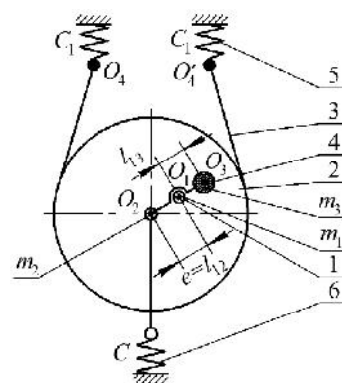


Figure 2. Initial position of the oscillating system: 1 – the vibrational exciter's drive shaft; 2 – roller; 3 – elastic band; 4 – counterweight; 5 – elastic support; 6 – vibration damper.

any oscillating movements. For this purpose, we shall select and display on the equivalent diagram a fixed Cartesian coordinate system O_2xy , the starting point of which is O_2 which is located at the roller's centre (in its initial position), while the axis O_2x is directed horizontally towards the right, and the axis O_2y is directed vertically towards the upwards position.

The equivalent diagram in Fig. 3 displays the following indicators: x_1 – linear horizontal offset for a drive shaft's centre of mass from the balance position; y_1 – linear vertical offset for a drive shaft's centre of mass from the balance position; φ_1 – angle of rotation for the vibrational exciter's drive shaft from the balance position; x_i, y_i – coordinates for point O_4 when attaching the left-hand end of the belt to the left-hand elastic support in a random position; or, x_r, y_r – coordinates for point O'_4 when attaching the right-hand end of the belt to the right-hand elastic support in a random position.

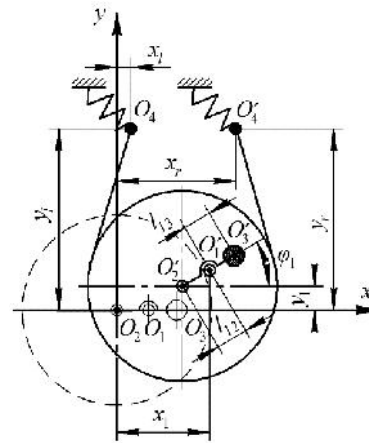


Figure 3. An equivalent diagram for the oscillating system in which the roller's centre of mass is offset from the balance position.

Furthermore, we shall create the differential equations for the movement of the oscillating system being discussed, utilising Type II Lagrange equations for this very purpose.

Within this context it has to be noted that the aforementioned oscillating system is characterised by three degrees of freedom: the linear shifts x_1, y_1 of a drive shaft's centre of mass (point O_1) in relation to the axes of the coordinates O_2x and O_2y , respectively, and the rotational angle φ_1 of the vibrational exciter's drive shaft (measured from the balance position).

RESULTS AND DISCUSSION

It must also be noted that the oscillating system incorporates three masses: m_1 – a drive shaft's mass; m_2 – a roller's mass; m_3 – a counterweight's mass.

To be able to establish the differential equations of movement by means of the aforementioned method, we shall first determine the kinetic energy of the oscillating system.

It is evident that the summary kinetic energy T of the oscillating system equals:

$$T = T_1 + T_2 + T_3, \quad (1)$$

where T_1 – is the kinetic energy of the translational movement of a drive shaft; T_2 – is the kinetic energy of the parallel plane movement of a roller; T_3 – is the kinetic energy of the parallel plane movement of a counterweight.

Within that context, the kinetic energy T_1 equals:

$$T_1 = \frac{m_1 V_1^2}{2}, \quad (2)$$

where m_1 – is a drive shaft's mass; V_1 – is a drive shaft's translational movement's speed.

The kinetic energy T_2 of a roller's parallel plane movement is determined as the kinetic energy of the module O_1O_2 , namely:

$$T_2 = \frac{m_2 V_2^2}{2} + \frac{I_2 \omega_1^2}{2}, \quad (3)$$

where m_2 – is the mass of a roller (module O_1O_2); V_2 – is the speed of the translational movement of a roller (module O_1O_2); ω_1 – is the angular velocity of a drive shaft; I_2 – is the moment of inertia in a roller (module O_1O_2) in relation to the point O_1 .

The kinetic energy T_3 is determined as the kinetic energy of the module O_1O_3 in its parallel plane of movement:

$$T_3 = \frac{m_3 V_3^2}{2} + \frac{I_3 \omega_1^2}{2}, \quad (4)$$

where m_3 – is the mass of a counterweight (module O_1O_3); V_3 – is the translational movement's speed of a counterweight (module O_1O_3); ω_1 – is the angular velocity of a drive shaft; I_3 – is the moment of inertia of a counterweight (module O_1O_3) in relation to the point O_1 .

Furthermore, we shall determine the kinetic characteristics (linear and angular velocities) of the points and modules of the moving masses m_1 , m_2 and m_3 .

It is evident that, within the coordinate system of O_2xy , the square of speed V_1 is:

$$V_1^2 = \dot{x}_1^2 + \dot{y}_1^2 \quad (5)$$

To determine the speeds V_2 and V_3 , we shall establish calculation diagrams for the modules O_1O_2 and O_1O_3 , making parallel plane movements. These calculation diagrams are provided in Fig. 4.

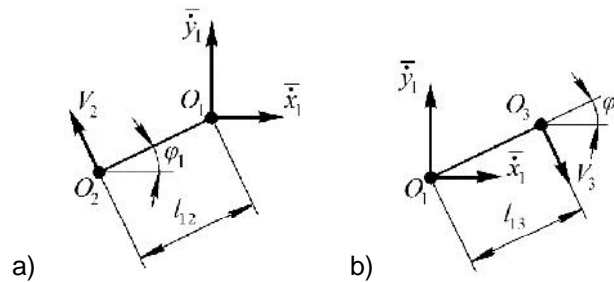


Figure 4. Calculation diagrams to determine the speeds of the oscillating system's modules: a) module O_1O_2 ; b) module O_1O_3 .

As the provided calculation diagrams indicate, the following expressions are yielded for the speed V_2 . The vector form of this is:

$$\vec{V}_2 = \vec{V}_1 + \vec{V}_{21} \quad (6)$$

Considering that the value of the speed V_{21} equals:

$$V_{21} = l_{12} \cdot \dot{\varphi}_1 \quad (7)$$

and after a number of translations, we get to the following:

$$V_2^2 = V_1^2 + 2l_{12} \cdot \dot{\varphi}_1 (0.5 \cdot l_{12} \cdot \dot{\varphi}_1 - \dot{x}_1 \cos \varphi_1 - \dot{y}_1 \sin \varphi_1). \quad (8)$$

Similarly, from the calculation diagram in Fig. 4, the expression for the speed V_3 is ultimately:

$$V_3^2 = V_1^2 + 2l_{13} \cdot \dot{\varphi}_1 (0.5 \cdot l_{13} \cdot \dot{\varphi}_1 + \dot{x}_1 \cos \varphi_1 + \dot{y}_1 \sin \varphi_1) \quad (9)$$

Furthermore, we shall determine the moments of inertias I_1 and I_2 of the modules O_1O_2 and O_1O_3 , in relation to a drive shaft's axis (point O_1), which are, respectively:

$$I_2 = m_2 \cdot l_{12}^2 \quad (10)$$

$$I_3 = m_3 \cdot l_{13}^2 \quad (11)$$

Inserting the expressions (5), (8) – (11) into the expressions (2), (3), (4), we get the following expressions for the relevant kinetic energies:

$$T_1 = \frac{m_1 (\dot{x}_1^2 + \dot{y}_1^2)}{2} \quad (12)$$

$$T_2 = \frac{m_2}{2} [\dot{x}_1^2 + \dot{y}_1^2 + 2l_{12} \cdot \dot{\varphi}_1 (0.5l_{12} \cdot \dot{\varphi}_1 - \dot{x}_1 \cos \varphi_1 - \dot{y}_1 \sin \varphi_1)], \quad (13)$$

and

$$T_3 = \frac{m_3}{2} [\dot{x}_1^2 + \dot{y}_1^2 + 2l_{13} \cdot \dot{\varphi}_1 (0.5l_{12} \cdot \dot{\varphi}_1 + \dot{x}_1 \cos \varphi_1 + \dot{y}_1 \sin \varphi_1)]. \quad (14)$$

Inserting the expressions (12), (13) and (14) into the expression (1), we get the expression for determining the summary kinetic energy of the oscillating system:

$$T = 0.5 \cdot (m_1 + m_2 + m_3) \cdot (\dot{x}_1^2 + \dot{y}_1^2) + m_2 \cdot l_{12} \cdot \dot{\varphi}_1 (0.5 \cdot l_{12} \cdot \dot{\varphi}_1 - \dot{x}_1 \cos \varphi_1 - \dot{y}_1 \sin \varphi_1) + m_3 \cdot l_{13} \cdot \dot{\varphi}_1 (0.5 \cdot l_{13} \cdot \dot{\varphi}_1 + \dot{x}_1 \cos \varphi_1 + \dot{y}_1 \sin \varphi_1) + 0.5(m_2 \cdot l_{12}^2 + m_3 \cdot l_{13}^2) \cdot \dot{\varphi}_1^2. \quad (15)$$

To determine the generalised forces that are included on the right-hand side of the Type II Lagrange equation, it is necessary to establish an equivalent diagram of forces for the oscillating system that is being studied (Fig. 5).

This equivalent diagram indicates the following forces and inertias:

- \bar{G}_1 – the force of a drive shaft's weight;
- \bar{G}_2 – the force of a working roller's weight;
- \bar{G}_3 – the force of a counterweight's weight;
- \bar{S}_1 – the tensioning force of the elastic belt's left-hand section;
- \bar{S}_2 – the tensioning force of the elastic belt's right-hand section;
- \bar{M}_T – the torque moment in a drive shaft.

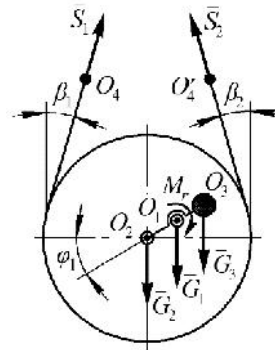


Figure 5. An equivalent diagram of forces in the oscillating system that is being studied.

Additionally, the diagram indicates:

φ_1 – the turning angle of a drive shaft;

β_1 – the angle between the elastic belt's left-hand section and the vertical;

β_2 – the angle between the elastic belt's right-hand section and the vertical.

Furthermore, we shall enter the expression that will be used to determine all forces and moments indicated into the equivalent diagram of Fig. 5:

$$G_1 = m_1 \cdot g, \quad (16)$$

where m_1 – a drive shaft's mass; g – gravitational acceleration;

$$G_2 = m_2 \cdot g, \quad (17)$$

where m_2 – is a roller's mass;

$$G_3 = m_3 \cdot g, \quad (18)$$

where m_3 – is a counterweight's mass.

The belt's tensioning forces S_1 and S_2 are equivalent to the elastic forces occurring upon the deformation of the elastic elements; therefore we shall determine them as follows:

$$S_1 = C_1 \cdot \Delta l_1 \quad (19)$$

$$S_2 = C_1 \cdot \Delta l_2 \quad (20)$$

where C_1 – is an elastic support's levels of 'hardness'; Δl_1 and Δl_2 – is the linear deformations of the left-hand and right-hand elastic support respectively.

The deformations Δl_1 and Δl_2 in the elastic elements are determined on the basis of a geometric analysis in the oscillating system.

As a result:

$$S_1 = C_1 \left(\sqrt{(x_l - x_l - l_{12} \cdot \sin \varphi_1)^2 + (y_l - y_l - l_{12} \cdot \cos \varphi_1)^2} - R^2 - \sqrt{x_l^2 + y_l^2 - R^2} \right), \quad (21)$$

and

$$S_2 = C_1 \left(\sqrt{(x_r - x_l + l_{12} \cdot \sin \varphi_1)^2 + (y_r - y_l - l_{12} \cdot \cos \varphi_1)^2} - R^2 - \sqrt{x_r^2 + y_r^2 - R^2} \right), \quad (22)$$

where R – is a roller's radius.

Next we shall determine the generalised forces in the oscillating system, corresponding to each of the independent generalised coordinates.

For the generalised coordinate φ_1 , the generalised force Q_{φ_1} is equal to the arithmetic sum of the moments of all forces in relation to the point O_1 , namely:

$$Q_{\varphi_1} = M_r - (G_2 \cdot l_{12} - G_3 \cdot l_{13}) \cos \varphi_1 + S_1 (R + l_{12}) \cdot \sin (\varphi_1 + \beta_1) - S_2 (R + l_{12}) \cdot \sin (\varphi_1 - \beta_1). \quad (23)$$

For the generalised coordinate x_1 , the generalised force Q_{x_1} is equal to the arithmetic sum of the projections of all forces indicated in Fig. 5 on the axis O_2x , namely:

$$Q_{x_1} = S_1 \cdot \sin \beta_1 - S_2 \cdot \sin \beta_2 - C_x \cdot x_1 \quad (24)$$

where C_x – is a vibration damper's hardness in the direction of the axis O_2x , and x_1 – is a vibration damper's linear deformation in the direction of the axis O_2x .

For the generalised coordinate y_1 , the generalised force Q_{y_1} is equal to the arithmetic sum of the projections of all forces indicated in Fig. 5 on the axis O_2y , namely:

$$Q_{y_1} = S_1 \cdot \cos \beta_1 + S_2 \cdot \cos \beta_2 - C_y (y_1 - \delta_{st}) - G_1 - G_2 - G_3 \quad (25)$$

where C_y – is a vibration damper's levels of 'hardness' in the direction of the axis O_2y ; y_1 – is a vibration damper's linear deformation in the direction of the axis O_2y ; and δ_{st} – is a vibration damper's static deformation.

In this way, the generalised forces are determined for each generalised coordinate of this oscillating system.

In addition, we shall determine the necessary partial differentiations of the kinetic energy T in this oscillating system which corresponds to the conditions that are contained in the left-hand sections of the Type II Lagrange equations. We get the following expression for the partial differentiation of the generalised coordinate ϕ_1 :

$$\begin{aligned} \frac{\partial T}{\partial \dot{\phi}_1} = & m_2 \cdot l_{12} (0.5 \cdot l_{12} \cdot \dot{\phi}_1 - \dot{x}_1 \cdot \cos \phi_1 - \dot{y}_1 \cdot \sin \phi_1) + \\ & + 0.5 \cdot m_2 \cdot l_{12}^2 \cdot \dot{\phi}_1 + m_3 \cdot l_{13} (0.5 \cdot l_{13} \cdot \dot{\phi}_1 + \dot{x}_1 \cdot \cos \phi_1 + \dot{y}_1 \cdot \sin \phi_1) + \\ & + 0.5 \cdot m_3 \cdot l_{13}^2 \cdot \dot{\phi}_1 + (m_2 \cdot l_{12}^2 + m_3 \cdot l_{13}^2) \cdot \dot{\phi}_1 ; \end{aligned} \quad (26)$$

also:

$$\begin{aligned} \frac{d}{dt} \left(\frac{\partial T}{\partial \dot{\phi}_1} \right) = & m_2 \cdot l_{12} (0.5 \cdot l_{12} \cdot \ddot{\phi}_1 - \ddot{x}_1 \cdot \cos \phi_1 + \dot{x}_1 \cdot \sin \phi_1 \cdot \dot{\phi}_1 - \\ & - \ddot{y}_1 \cdot \sin \phi_1 - \dot{y}_1 \cdot \cos \phi_1 \cdot \dot{\phi}_1) + 0.5 \cdot m_2 \cdot l_{12}^2 \cdot \ddot{\phi}_1 + \\ & + m_3 \cdot l_{13} (0.5 \cdot l_{13} \cdot \ddot{\phi}_1 + \ddot{x}_1 \cdot \cos \phi_1 - \dot{x}_1 \cdot \sin \phi_1 \cdot \dot{\phi}_1 + \\ & + \ddot{y}_1 \cdot \sin \phi_1 + \dot{y}_1 \cdot \cos \phi_1 \cdot \dot{\phi}_1) + 0.5 \cdot m_3 \cdot l_{13}^2 \cdot \ddot{\phi}_1 + (m_2 \cdot l_{12}^2 + m_3 \cdot l_{13}^2) \cdot \ddot{\phi}_1 = \\ = & 0.5 \cdot m_2 \cdot l_{12}^2 \cdot \ddot{\phi}_1 + m_2 \cdot l_{12} (-\ddot{x}_1 \cdot \cos \phi_1 + \dot{x}_1 \cdot \sin \phi_1 \cdot \dot{\phi}_1 - \\ & - \ddot{y}_1 \cdot \sin \phi_1 - \dot{y}_1 \cdot \cos \phi_1 \cdot \dot{\phi}_1) + 0.5 \cdot m_2 \cdot l_{12}^2 \cdot \ddot{\phi}_1 + \\ & + 0.5 \cdot m_3 \cdot l_{13}^2 \cdot \ddot{\phi}_1 + m_3 \cdot l_{13} (\ddot{x}_1 \cdot \cos \phi_1 - \dot{x}_1 \cdot \sin \phi_1 \cdot \dot{\phi}_1 + \ddot{y}_1 \cdot \sin \phi_1 + \\ & + \dot{y}_1 \cdot \cos \phi_1 \cdot \dot{\phi}_1) + 0.5 \cdot m_3 \cdot l_{13}^2 \cdot \ddot{\phi}_1 + (m_2 \cdot l_{12}^2 + m_3 \cdot l_{13}^2) \cdot \ddot{\phi}_1 = \\ = & 2(m_2 \cdot l_{12}^2 + m_3 \cdot l_{13}^2) \cdot \ddot{\phi}_1 + m_2 \cdot l_{12} (-\ddot{x}_1 \cdot \cos \phi_1 + \dot{x}_1 \cdot \sin \phi_1 \cdot \dot{\phi}_1 - \\ & - \ddot{y}_1 \cdot \sin \phi_1 - \dot{y}_1 \cdot \cos \phi_1 \cdot \dot{\phi}_1) + m_3 \cdot l_{13} (\ddot{x}_1 \cdot \cos \phi_1 + \dot{x}_1 \cdot \sin \phi_1 \cdot \dot{\phi}_1 + \\ & + \ddot{y}_1 \cdot \sin \phi_1 + \dot{y}_1 \cdot \cos \phi_1 \cdot \dot{\phi}_1). \end{aligned} \quad (27)$$

The partial differentiation of the kinetic energy of the generalised coordinate ϕ_1 is:

$$\begin{aligned} \frac{\partial T}{\partial \phi_1} = & m_2 \cdot l_{12} \cdot \dot{\phi}_1 (\dot{x}_1 \cdot \sin \phi_1 - \dot{y}_1 \cdot \cos \phi_1) + \\ & + m_3 \cdot l_{13} \cdot \dot{\phi}_1 (-\dot{x}_1 \cdot \sin \phi_1 + \dot{y}_1 \cdot \cos \phi_1). \end{aligned} \quad (28)$$

For the generalised coordinate x , we get the following expressions of partial differentiations in the oscillating system's kinetic energy T :

$$\frac{\partial T}{\partial \dot{x}_1} = (m_1 + m_2 + m_3) \cdot \dot{x}_1 - m_2 \cdot l_{12} \cdot \dot{\varphi}_1 \cdot \cos \varphi_1 + m_3 \cdot l_{13} \cdot \dot{\varphi}_1 \cos \varphi_1 \quad (29)$$

also:

$$\begin{aligned} \frac{d}{dt} \left(\frac{\partial T}{\partial \dot{x}_1} \right) &= (m_1 + m_2 + m_3) \cdot \ddot{x}_1 - m_2 \cdot l_{12} \cdot \ddot{\varphi}_1 \cdot \cos \varphi_1 + \\ &+ m_2 \cdot l_{12} \cdot \sin \varphi_1 \cdot \dot{\varphi}_1^2 + m_3 \cdot l_{13} \cdot \ddot{\varphi}_1 \cdot \cos \varphi_1 - m_3 \cdot l_{13} \cdot \dot{\varphi}_1^2 \cdot \sin \varphi_1 ; \end{aligned} \quad (30)$$

and finally:

$$\frac{\partial T}{\partial x_1} = 0 \quad (31)$$

For the generalised coordinate y_1 , we get the following expressions of partial differentiations in the kinetic energy T :

$$\frac{\partial T}{\partial \dot{y}_1} = (m_1 + m_2 + m_3) \cdot \dot{y}_1 - m_2 \cdot l_{12} \cdot \dot{\varphi}_1 \cdot \sin \varphi_1 + m_3 \cdot l_{13} \cdot \dot{\varphi}_1 \sin \varphi_1 \quad (32)$$

also:

$$\begin{aligned} \frac{d}{dt} \left(\frac{\partial T}{\partial \dot{y}_1} \right) &= (m_1 + m_2 + m_3) \cdot \ddot{y}_1 - m_2 \cdot l_{12} \cdot \ddot{\varphi}_1 \cdot \sin \varphi_1 - \\ &- m_2 \cdot l_{12} \cdot \cos \varphi_1 \cdot \dot{\varphi}_1^2 + m_3 \cdot l_{13} \cdot \ddot{\varphi}_1 \cdot \sin \varphi_1 + m_3 \cdot l_{13} \cdot \dot{\varphi}_1^2 \cdot \cos \varphi_1 ; \end{aligned} \quad (33)$$

and finally:

$$\frac{\partial T}{\partial y_1} = 0 ; \quad (34)$$

When inserting the resulting expressions (23), (24), (25), (27), (28), (30), (31), (33) and (34) into the initial Type II Lagrange equation for each generalised coordinate and performing the required translations, we get the following system of differential equations for the oscillating system's movement:

$$\left. \begin{aligned} 2(m_2 \cdot l_{12}^2 + m_3 \cdot l_{13}^2) \ddot{\varphi} &= -m_2 \cdot l_{12} \{ -\ddot{x}_1 \cdot \cos \varphi_1 + \dot{x}_1 \cdot \sin \varphi_1 \cdot \dot{\varphi}_1 - \\ &- \ddot{y}_1 \cdot \sin \varphi_1 - \dot{y}_1 \cdot \cos \varphi_1 \cdot \dot{\varphi}_1 \} - m_3 \cdot l_{13} \{ \ddot{x}_1 \cdot \cos \varphi_1 - \dot{x}_1 \cdot \sin \varphi_1 \cdot \dot{\varphi}_1 + \\ &+ \ddot{y}_1 \cdot \sin \varphi_1 + \dot{y}_1 \cdot \cos \varphi_1 \cdot \dot{\varphi}_1 \} + m_2 \cdot l_{12} \cdot \dot{\varphi}_1 \{ \dot{x}_1 \cdot \sin \varphi_1 - \dot{y}_1 \cdot \cos \varphi_1 \} + \\ &+ m_3 \cdot l_{13} \cdot \dot{\varphi}_1 \{ -\dot{x}_1 \cdot \sin \varphi_1 + \dot{y}_1 \cdot \cos \varphi_1 \} + M_r - (m_2 \cdot l_{12} - \\ &- m_3 \cdot l_{13}) \cdot g \cdot \cos \varphi_1 + S_1 (R + l_{12}) \cdot \sin (\varphi_1 + \beta_1) - S_2 (R + l_{12}) \cdot \sin (\varphi_1 - \beta_1), \\ \\ (m_1 + m_2 + m_3) \ddot{x}_1 &= m_2 \cdot l_{12} \cdot \ddot{\varphi}_1 \cdot \cos \varphi_1 - m_2 \cdot l_{12} \cdot \sin \varphi_1 \cdot \dot{\varphi}_1^2 - \\ &- m_3 \cdot l_{13} \cdot \ddot{\varphi}_1 \cdot \cos \varphi_1 + m_3 \cdot l_{13} \cdot \sin \varphi_1 \cdot \dot{\varphi}_1^2 + S_1 \cdot \sin \beta_1 - S_2 \cdot \sin \beta_2 - C_x \cdot x_1, \\ \\ (m_1 + m_2 + m_3) \ddot{y}_1 &= m_2 \cdot l_{12} \cdot \ddot{\varphi}_1 \cdot \sin \varphi_1 + m_2 \cdot l_{12} \cdot \cos \varphi_1 \cdot \dot{\varphi}_1^2 - \\ &- m_3 \cdot l_{13} \cdot \ddot{\varphi}_1 \cdot \sin \varphi_1 - m_3 \cdot l_{13} \cdot \cos \varphi_1 \cdot \dot{\varphi}_1^2 + S_1 \cdot \cos \beta_1 + S_2 \cdot \cos \beta_2 - \\ &- C_y (y_1 - \delta_{st}) - (m_1 + m_2 + m_3) g. \end{aligned} \right\} \quad (35)$$

This system of differential equations (35) is one that involves non-linear differential equations of Type II, and can be solved using digital methods on a PC such as, for example, with the MathCAD software.

The initial conditions for the system of differential equations are as follows:

If $t = 0$:

$$x_{10} = l_{12}, y_0 = 0, \dot{x}_{10} = 0, \dot{y}_{10} = 0, \text{ and } \varphi_{10} = 0 \quad (36)$$

For digital calculations in the MathCAD software, the following values were set up for the constant parameters that were included in the system for differential equations (35). Based on the calculations that have been recorded during the design and subsequent manufacture of the experimental specimen of the infrared dryer, but also based on the results of testing and redesigning the dryer, the following values have been taken for constant parameters:

- a drive shaft's mass $m_1 = 5.4$ kg;
- a roller's mass $m_2 = 6.2$ kg;
- a counterweight's mass $m_3 = 1.2$ kg;
- the distance from a drive shaft's axis to a roller's axis (the offset rate) $l_{12} = 0.003$ m;
- the distance from a drive shaft's axis to a counterweight's axis is determined by this condition. From $m_3 \cdot l_{13} = m_1 \cdot l_{12}$, the following results:

$$l_{13} = \frac{m_1 \cdot l_{12}}{m_3} = \frac{5.4 \cdot 0.003}{1.2} = 0.0135 \text{ m}$$

On the basis of our designing, manufacturing, and testing the new type of vibrational dryer with its vibrational wave transporter belt, which confirmed its functioning, we also take the following values as constants for the following parameters:

- a vibration damper's 'hardness' in the direction of the axis O_2x : $C_x = 9,800$ N m⁻¹
- a vibration damper's 'hardness' in the direction of the axis O_2y : $C_y = 31,000$ N m⁻¹;
- a drive shaft's rotational moment $M_r = 4.2$ kNm.

The digital calculations for the system of differential equations as carried out on a PC (35) provided dependencies for the movement (trajectory) of the rollers along the axis of the coordinates O_2x and O_2y , as depicted in Fig. 6.

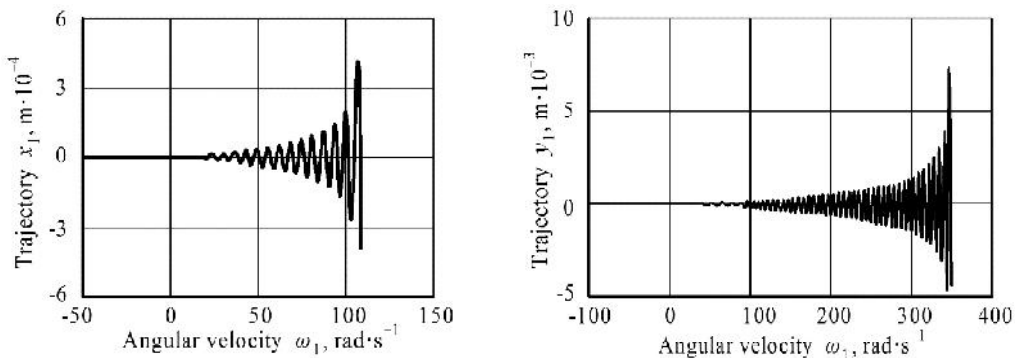


Figure 6. The trajectories of a roller's centre of mass along the coordinates O_2x , O_2y , depending on the angular velocity ω_1 .

We also used digital modelling on a PC to get the dependence of the excitation force F_d on the angular velocity ω_1 (Fig. 7) and also the dependence of the power consumption N on the angular velocity ω_1 (Fig. 8).

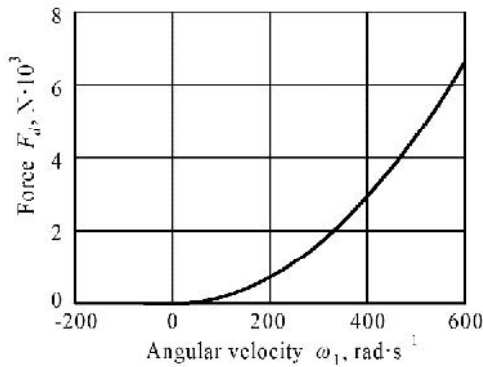


Figure 7. The dependence of the excitation force F_d on the angular velocity ω_1 .

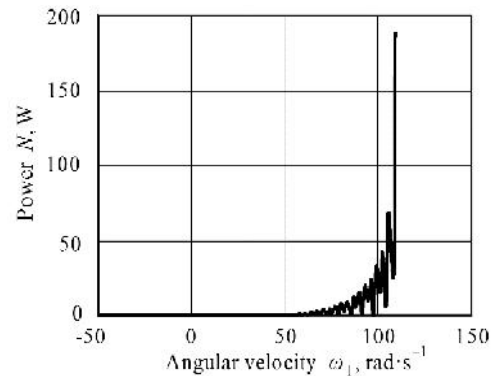


Figure 8. The dependence of the consumer power figure N on the angular velocity ω_1 .

As the graphs in Fig. 6 indicate, a stable oscillating movement in a roller takes place when changing a drive shaft's angular speed ω_1 within the range of 100–120 rad s^{-1} . With that occurring, a roller's oscillation amplitude changes within the limits of $1.0\text{--}4.0 \cdot 10^{-3}$ m in the direction of the axis O_2x and within the limits of $1.0\text{--}2.0 \cdot 10^{-3}$ m in the direction of the axis O_2y , which ensures the generation of a necessary wave on the elastic belt's surface, ie. the necessary vibrational wave-type movement of the bulk grain along the elastic belt's surface, simultaneously with the bulk grain being mixed under the infrared radiator that is drying the bulk grain.

The graphical dependencies pictured in Fig. 7 indicate that the value of the excitation force F_d starts increasing significantly (going above $1 \cdot 10^3$ N) if a drive shaft's angular velocity ω_1 is increased to 220 rad s^{-1} . At a drive shaft's angular velocity ω_1 reaching 120 rad s^{-1} , the value of the aforementioned force does not exceed 350 N (0.35 kN). Therefore, when considering the reliability of the vibrational exciter, it is not recommended that the angular velocity ω_1 be increased above 120 rad s^{-1} , because the power consumption level may increase to infinity.

Moreover, the graphs in Fig. 8 indicate that, upon increasing a drive shaft's angular velocity ω_1 to 120 rad s^{-1} , the power consumption level of the vibrational exciter reached 50 W, which is more acceptable in a situation which requires minimum energy spend in return for the high quality performance of the technological process.

Therefore, all of the graphs that have been discussed above indicate that the rational values for the angular velocity ω_1 of the vibrational exciter's drive shaft must fall within the range of 100–120 rad s^{-1} .

We also carried out experimental studies to investigate the process involved in the infrared drying of soy seeds on a vibrational transporter that had been developed by us.

An experimental installation was established on the basis of that concept, and a diagram of it is provided in Fig. 9. The operating principle of the experimental installation is similar to that of the industrial model of an infrared dryer with a novel design, incorporating into it a vibrational belt transporter.

In the course of the experimental studies, portions of soy seeds with fixed moisture parameters were taken out at moisture levels of between 0.1% to 7.0%. The speed at which the bulk grain was being transported was also set at levels of between 0.15 to 0.6 $\text{cm}\cdot\text{s}^{-1}$. The time spent by each portion of the seeds under the infrared lamps was recorded. The data received from this enabled us to determine the drying speed (the speed at which moisture is removed). For each portion of the seeds and to ensure individually-noted transportation speed readings, triple tests were carried out. The measurement and calculation results were processed with specially developed software on a PC.

Based on the results of the experimental studies, the speed at which the soy seed can be dried in the aforementioned dryer was all assessed. The experimental data was used to prepare a table which indicated the data of the infrared drying speed (removing moisture from the dried bulk grain over time) at various speeds of transporting the bulk grain on the vibrational belt and at various levels of moisture content in the bulk grain (Table 1).

The details given in the table indicates that the speed of infrared drying (moisture removal) for bulk seed depends upon both its initial moisture content and the speed of its vibrational transport. Within that context, the drying time for the bulk grain also changes. At a constant speed of vibrational transport for bulk grain, and with an increase of its initial relative moisture content, the time actually lengthens for the stage at which a constant drying speed can be achieved for drying soy seeds. As can be seen from the table above, for a vibrational transportation speed of 0.15 cm s^{-1} , when the relative moisture content changes from 0.70% to 6.80%, the time needed to attain a constant speed of $12.1\text{--}13.2\cdot 10^{-3} \text{ \%}\cdot\text{s}^{-1}$ in terms of drying the bulk grain changes from 85 s to 520 s.

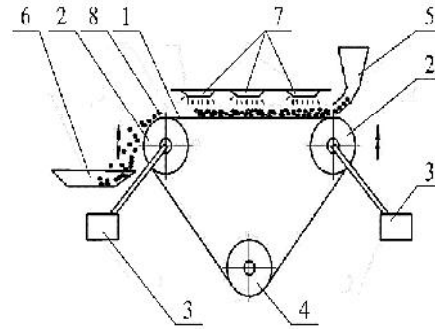


Figure 9. A diagram of an experimental installation in order to study the process of the infrared drying of soy seeds: 1) elastic belt; 2) rollers; 3) roller drive; 4) tensioning roller; 5) feeder hopper; 6) collector for dried seeds; 7) infrared radiator; 8) soy seeds.

at various speeds of transporting the bulk grain on the vibrational belt and at various levels of moisture content in the bulk grain (Table 1).

Table 1. Individual energy and technology parameters for the infrared drying of soy seeds

Specific moisture content of the seeds, $\Delta W, \%$	Speed of vibrational transportation of the seeds, $V, \text{cm s}^{-1}$	Drying time, τ, s	Speed at which moisture is removed, $dW\cdot(dt)^{-1}, \text{\%}\cdot\text{s}^{-1}\cdot 10^{-3}$
0.70	0.15	85	8.24
2.70	0.15	205	13.17
4.60	0.15	380	12.11
6.80	0.15	520	13,10
0.10	0.40	45	2.22
0.30	0.40	84	7.97
1.70	0.40	160	10.63
2.90	0.40	235	12.34
0.15	0.60	50	3.00
0.58	0.60	95	6.10
1.20	0.60	140	8.57
2.40	0.60	320	7.50

For a vibrational transportation speed of $0.40 \text{ cm}\cdot\text{s}^{-1}$, when changing the relative moisture level from 0.10% to 2.9% and when the drying speed stabilises at the level of $12.3\cdot 10^{-3} \text{ \%}\cdot\text{s}^{-1}$, the drying time for the soy seeds changes from 45 s to 235 s.

And finally, at a vibrational transportation speed of $0.60\text{cm}\cdot\text{s}^{-1}$ and with the drying time as set out in the table, the drying speed for soy deeds does not exceed $8.6\cdot 10^{-3} \text{ \%}\cdot\text{s}^{-1}$, ie. a drying speed level of $12\cdot 10^{-3} \text{ \%}\cdot\text{s}^{-1}$ is not attained in this case.

Therefore, based on the data gained from the experimental studies that have been carried out here, a rational speed for the vibrational transportation of soy seeds in infrared drying falls within the range of between 0.15 to 0.40 cm s^{-1} .

CONCLUSIONS

1. A thermal radiation dryer of a novel design has been developed using a vibrational wave transport element which generates a mechanical wave on the surface of the flexible transporter belt, which itself ensures the movement of bulk grain along the processing zone that is currently being treated with infrared radiation.

2. On the basis of the calculation diagrams that have been developed, a mathematical model was prepared of the vibrational process that was the subject of the study, namely involving the use of Type II Lagrange equations which resulted in a system of differential equations for the movement of the vibrational exciter with its novel design, as proposed by the authors.

3. The solving of the aforementioned integral equations on a PC yielded a number of graphical dependencies for the kinetic and dynamic parameters of the vibrational system that has been described above.

4. It has been demonstrated that the stable movement of a working roller takes place if the angular velocity ω_1 is changed within the range of $100\text{--}120 \text{ rad s}^{-1}$, while the rational amplitude of the vibrational exciter's oscillations does not exceed 4 mm.

5. The fact has been identified that a rational speed for transporting soy seeds during infrared drying falls between the range of $0.15\text{--}0.60 \text{ cm s}^{-1}$. This parameter within the stated limits increases the time taken until the stage of constant drying speed can be achieved for soy by more than 2.5 times, from 205 s to 520 s, stabilising at a level of 520 s.

6. At a drive shaft's angular velocity ω_1 being 120 rad s^{-1} , the value of the excitation force F_d does not exceed 0.35 kN but, when it does actually exceed it, the excitation force starts increasing significantly.

7. When increasing a drive shaft's angular velocity ω_1 to 120 rads^{-1} , the power consumption of the vibrational exciter reached 50W, which again confirms the finding that the rational range when it comes to changing a drive shaft's angular velocity falls between $100\text{--}120 \text{ rad s}^{-1}$.

8. As shown by the results of the experimental studies that have been conducted, a rational speed for the vibrational transportation of soy seeds in infrared drying falls between 0.15 to 0.40 cm s^{-1} .

REFERENCES

Aboltins, A. & Upitis, A. 2012. Experimental and theoretical investigation of agricultural material drying process. *Engineering for Rural Development* **11**, 93–98.

- Bezbakh, I.V. & Bakhmutyan, N.V. 2006. Investigation of the drying process of fruits and berries in a suspended layer. *Scientific works of ONAHT*, Odessa, **28**, pp. 112–116.
- Boyce, D.S. 1965. Grain moisture and temperature changes with position and time during through drying. *Journal of Agricultural Engineering Research* **10**(4), 333–341. doi: 10.1016/0021-8634(65)90080-6
- Bruce, D.M. & Giner, S.A. 1993. Mathematical modelling of grain drying counter-flou beds: Investigation of crossover of air and grain temperatures. *Journal of Agricultural Engineering Research* **55**(2), 143–161. doi: 10.1006/jaer.1993.1039
- El Hor, H., Linz, S.J., Grochowski, R., Walzel, P., Kruelle, C.A., Rouijaa, M., Götzendorfer, A. & Rehberg, I. 2005. Model for transport of granular matter on vibratory conveyors. *Powders and Grains 2005 - Proceedings of the 5th International Conference on Micromechanics of Granular Media* **2**, 1191–1195.
- Filonenko, G.K. & Grishin, M.A. 1971. *Drying of food plant materials*. Moscow, Food Industry, 231 pp. (in Russian)
- Gilmore, C., Asefi, M., Nemez, K., Paliwal, J. & LoVetri, J. 2019. Three dimensional radio-frequency electromagnetic imaging of an in.bin grain conditioning process. *Computers and Electronics in Agriculture* **167**, Article no. 105059. doi:10.1016/j.compag.2019.105059
- Giner, S.A. 2019. Estimation of the influence of variable boundary when using thin layer equations for grain dryer simulation. *Biosystems Engineering* **186**, 228–233. doi: 10.1016/j.biosystemseng.2019.08.004
- Goncharevich, I.F. & Frolov, K.V. 1981. *The theory of vibration technique and technology*. Moscow: Nauka, 217 pp. (in Russian).
- Grochowski, R., Walzel, P., Rouijaa, M., Kruelle, C.A. & Rehberg, I. 2004. Revising granular flow on a vibratory conveyor. *Applied Physics Letter* **84**(6), 1019–1021. doi: 10.1063/1.1646219
- Hemis, M., Choudhary, R. & Watson, D.G. 2012. A coupled mathematical model for simultaneous microwave and convective drying of wheat seeds. *Biosystems Engineering* **112**(3), 202–209. doi: 10.1016/j.biosystemseng.2012.04.002
- Kliuchnikov, A. 2019. Development of new method of drying at energy-saving universal dryer to improve quality of crops used in fodder production. *Engineering for Rural Development* **18**, 105–111. doi: 10.22616/ERDev2019.18.N125
- Malin, N.I. 2005. *Grain storage technology*. Moscow, Kolos, 280 pp.
- Moroz, S.M., Vasilkovsky, M.I., Vasilkovsky, O.M. & Goncharov, V.V. 2011. Analysis of the multilayer movement of grain on a fixed working surface. *Design, production and operation of agricultural machinery, Proceedings of Kirovograd National Technical University, Kirovograd*, **41**, pp. 203–208.
- Mujumar, A.S. 1995. *Handbook of Industrial Drying*, New York: Dekker, 742 pp.
- Palamarchuk, I.P., Kurchev, S.V. & Verkholtantseva, V.A. 2018. Trends in the development of conveyor vibratory dryers. In: *The development of technical sciences: problems and solutions: Proceedings of the international research and practical conference (April, 27–28, 2018)*, Brno, pp. 9–12.
- Rogovskii, I.L., Titova, L.L., Trokhaniak, V.I., Solomka, O.V., Popyk, P.S., Shvidia, V.O. & Stepanenko, S.P. 2019. Experimental studies on druing conditions of grain crops with high moisture content in low-pressure environment. *INMATEH – Agricultural Engineering* **57**(1), 141–146.
- Rudobashta, S.P., Zueva, G.A. & Kartashov, E.M. 2016. Heat and mass transfer when drying a spherical particle in an oscillating electromagnetic field. *Theoretical Foundations of Chemical Engineering* **50**(5), 718–729. <http://www.kluweronline.com/issn/0040-5795>. doi: 10.1134/S0040579516050365
- Safarov A.F. 1991. *Moisture and thermal processing of oilseeds*. A Thesis for applying for the degree of Doctor in Engineering Sciences, Tashkent, 288 pp.